Supporting information for

Grasping Hydrogen Adsorption and Dynamics in Metal-Organic Frameworks Using ^{2}H Solid-State NMR

Bryan E.G. Lucier,[#] Yue Zhang,[#] Kelly J. Lee, Yuanjun Lu, Yining Huang*

Department of Chemistry, The University of Western Ontario, London, Ontario, Canada, N6A 5B7
*Corresponding author, E-mail: yhuang@uwo.ca
[#] These authors contributed equally to the manuscript.

Table of Contents

Experimental Section

MOF synthesis. All chemicals were obtained from Sigma-Aldrich and were used without further purification. Mg-MOF-74, Ni-MOF-74, Zn-MOF-74, UiO-66, α-$Mg_3(COOH)_6$, and α-$Zn_3(COOH)_6$ were synthesized using previously described methods, which are detailed below.[1-6]

Mg-MOF-74. 0.75 mmol (0.1486 g) of 2,5-dihydroxyterephthalic acid (H_4DOBDC) was dissolved in 10 mL tetrahydrofuran (THF) in a 23 mL Teflon-lined stainless steel autoclave. 3 mL of 1.0 M aqueous sodium hydroxide solution was then added to the reagent mixture. 1.5 mmol (0.3846 g) $Mg(NO_3)_2{\cdot}6H_2O$ was dissolved in 5 mL deionized water, and then added to the reagent mixture in the Teflon inlet while stirring. The reagent mixture was heated in the autoclave at 110 ^oC for 3 days. The powdered yellow product was washed three times with THF and dried using vacuum filtration.

Ni-MOF-74. 0.75 mmol (0.1486 g) of H_4DOBDC was first dissolved in 10 mL THF within a 23 mL Teflon-lined stainless steel autoclave. 1.5 mmol (0.3733 g) of $Ni(CH_3COO)_2{\cdot}4H_2O$ was dissolved in 5 mL deionized water and then added to the reagent mixture in the Teflon inlet. After 1 hour of stirring in ambient conditions, the autoclave was sealed, and the mixture was planed in a 110 °C oven for 3 days. The ochre (i.e., yellow-orange-brown) product was obtained as a powder, which was washed three times with THF and dried using vacuum filtration.

Zn-MOF-74. Both 10 mL of THF and 0.75 mmol (0.1486 g) of H_4DOBDC were added to a 23 mL Teflon-lined stainless steel autoclave. Once the H_4DOBDC was dissolved, 3 mL aqueous sodium hydroxide solution (1 M) was added to the reagent solution. 1.5 mmol (0.4462 g) $Zn(NO_3)_2 \cdot 6H_2O$ was first dissolved in 5 mL deionized water, and the resulting solution was added to the reagent mixture in the Teflon inlet while stirring. The reactants in the autoclave were heated at 110 ^oC for 3 days, yielding a powdered yellow-green product that was washed three times with THF and dried using vacuum filtration.

UiO-66. A mixture of 0.54 mmol (0.125 g) $ZrCl_4$, 5 mL *N*,*N*-dimethylformamide (DMF), and 1 mL concentrated HCl (ca. 12.1 M) were mixed together and sonicated for 20 minutes until fully dissolved. This mixture was then transferred to a 23 mL Teflon-lined stainless steel autoclave, along with 0.75 mmol (0.123 g) terephthalic acid (H_2BDC) and 10 mL DMF. The resulting reagent mixture was sonicated for another 20 minutes. The autoclave was then heated for 24 hours at 80 ^oC. The white product was obtained as a powder, which was washed three times with DMF, followed by another three times with ethanol. The product was dried using vacuum filtration.

α-$Mg_3(COOH)_6$. 3 mmol (0.7692 g) $Mg(NO_3)_2 \cdot 6H_2O$, 6 mmol (0.2762 g) formic acid (HCOOH), and 10 mL DMF were first mixed in a 23 mL Teflon-lined stainless steel autoclave and then heated at 110 ^oC for 2 days. The white crystalline product was washed with DMF and dried using vacuum filtration. α-$Zn_3(COOH)_6$ was prepared according to literature procedures,[6] using zinc nitrate and methanol.

Sample activation. In order to prepare activated (dehydrated) samples, the as-made Ni-MOF-74, Zn-MOF-74, UIO-66, α-$Mg_3(COOH)_6$, and α-$Zn_3(COOH)_6$ samples were heated at 150 ^oC under dynamic vacuum (*i.e.*, < 1 mbar) for 8 hours. For Mg-MOF-74, an additional solvent-exchange step was required to isolate a pure, activated MOF. 0.25 g of the as-made sample was solvent-exchanged by exposure to 10 mL of methanol in an autoclave at 200 ^{o}C for 7 days. Each day, the autoclave was removed from the oven, and the methanol stock was replaced. In the final step, the methanol exchanged Mg-MOF-74 sample was heated at 250 ^{o}C under dynamic vacuum for 8 hours.

Gas adsorption. A Schlenk line was used for gas adsorption experiments. The MOF sample was first loaded into the bottom of a homemade 5 mm L-shaped glass tube. A thin layer of glass wool was used to secure the sample in place. The glass tube was then attached to the Schlenk line, and sample activation was performed. A known amount of pressurized D_2 was then introduced to the vacuum line, and the D_2 was allowed to occupy both the vacuum line and the glass tube containing the sample (ca. 82.7 cm^3). The bottom of the D_2-filled glass tube was immersed in liquid nitrogen to freeze D_2 within the sample, and the glass tube was then flame-sealed from the Schlenk line. The overall D_2 loading amount is expressed by the molar ratio between D_2 and the metal. In this study, 0.2 D_2/metal samples were prepared for Ni-, Mg-, and Zn-MOF-74, while 0.1 D_2/metal samples were prepared for UiO-66, α-$Mg_3(COOH)_6$, and α-$Zn_3(COOH)_6$. For comparison purposes, a 0.1 D_2/metal sample of Mg-MOF-74 was also examined.

^{2}H solid-state NMR experiments. All solid-state NMR experiments were performed on a wide-bore Varian/Chemagnetics InfinityPlus NMR spectrometer operating at 9.4 T ($\upsilon_0(^2H)$ = 61.32 MHz) and equipped with a 5 mm static HX probe. A sample of D_2O (l) was used as a secondary chemical shift reference at δ_{iso} = 4.8 ppm with respect to neat $(CD_3)_4Si$.[7] The experimental temperature was controlled by a Varian VT control unit, and all temperatures were calibrated to ± 3 ° K using the ^{207}Pb chemical shift of a solid sample of lead nitrate across the experimental temperature range.[8] An quadrupolar echo pulse sequence of the format ($\pi/2 - \tau_1 - \pi/2 - \tau_2$) with Exorcycle phase cycling was used to acquire undistorted ^{2}H NMR spectra,[9] employing a $\pi/2$ pulse width of 1.8 μs, an interpulse τ_1 time of 30 μs, and a τ_2 period of 25 μs. A ^{1}H decoupling field of ca. 90 kHz was applied during all NMR experiments.

All spectra were acquired using calibrated ^{2}H pulse delays ranging from 1 to 3 s, depending on the experimental temperature. A spectral width of 200 kHz and acquisition time of 20.5 ms was employed for all ^{2}H NMR experiments, except those on Ni-MOF-74 at temperatures of 213 K and below, which used a spectral width of 400 kHz and an acquisition time of 10.25 ms. In addition, during NMR experiments on D_2 gas adsorbed in Ni-MOF-74, the transmitter position was also gradually moved from 61.325 MHz at room temperature to 61.396 MHz at 133 K in order to ensure complete excitation and detection of the broad ^{2}H powder pattern.

NMR parameters. The ^{2}H nucleus has a spin of 1, which means that ^{2}H has an electric quadrupole moment (Q) and is subject to the quadrupolar interaction (QI). The QI arises from the coupling between the electric quadrupole moment of ^{2}H and surrounding local electric field gradients (EFGs). The EFG may be modeled by a traceless tensor with three orthogonal components V_{11}, V_{22}, and V_{33}, where $|V_{11}| \leq |V_{22}| \leq |V_{33}|$. ^{2}H SSNMR spectra are dominated by the first-order quadrupolar interaction, which is described using two quantities. The quadrupolar coupling constant (C_Q) describes the local spherical symmetry about ^{2}H, and is defined such that $C_Q = (eQV_{33}/h) \times 9.7177 \times$

10^{21}; e is the fundamental electric charge, h is Planck's constant, V_{33} is the component of the EFG tensor that is largest in magnitude, and 9.7177×10^{21} is a conversion factor from atomic units to Hz. A large C_Q value is indicative of relatively low local symmetry, while low C_Q values are associated with ^{2}H environments of high symmetry and/or significant molecular dynamics. The asymmetry parameter, η_Q, corresponds to the degree of axial symmetry about ^{2}H, where $\eta_Q = (V_{11} - V_{22})/V_{33}$. A high η_Q value translates to low local axial symmetry, while a low η_Q value indicates that axial symmetry is largely preserved about ^{2}H. When ^{2}H resides in an environment of high local rotational symmetry (i.e., on a $\geq C_3$ rotational axis), η_Q is necessarily equal to zero.

Spectral simulations. The WSolids software program[10] was used to perform analytical simulations of experimental data and determine the observed, or apparent, NMR parameters. The error or uncertainty in NMR parameters was ascertained via bidirectional variation of each individual NMR parameter until noticeable discrepancies between the simulated and experimental spectra were apparent. The EXPRESS software[11] was used to simulate the effects of dynamic motion on the ^{2}H quadrupolar parameters and corresponding powder patterns, yielding the types and rates of motions present, along with their respective motional angles at all experimental temperatures.

Powder X-ray diffraction. The identity of all MOF products was confirmed through the use of powder XRD experiments, which were performed on an Inel CPS powder diffractometer operating with Cu Kα radiation. Reflections were collected at 2θ values ranging from 5 to 120 °. All pXRD patterns are depicted in Figure S12.

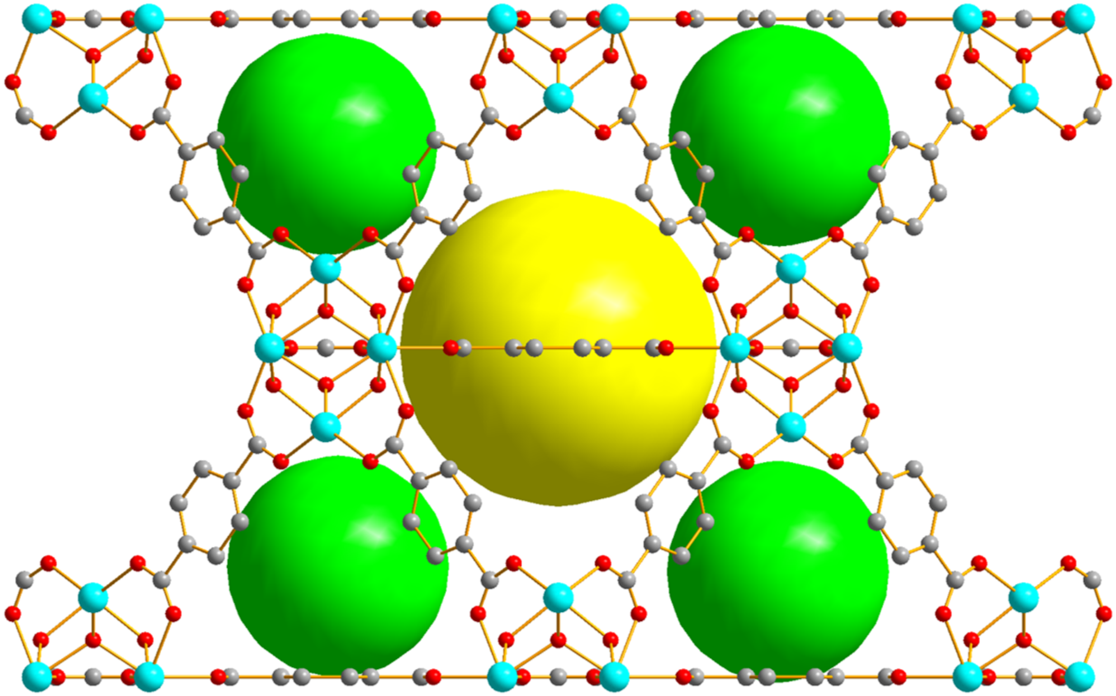

Figure S1. The structure of UiO-66 is shown, featuring octahedral cages highlighted by the larger yellow sphere. The face of each octahedral cage is shared with 8 smaller tetrahedral cages, denoted by relatively smaller green spheres. The colors red, grey and cyan correspond to oxygen, carbon and the zirconium metal center, respectively. Hydrogen atoms are omitted for clarity.

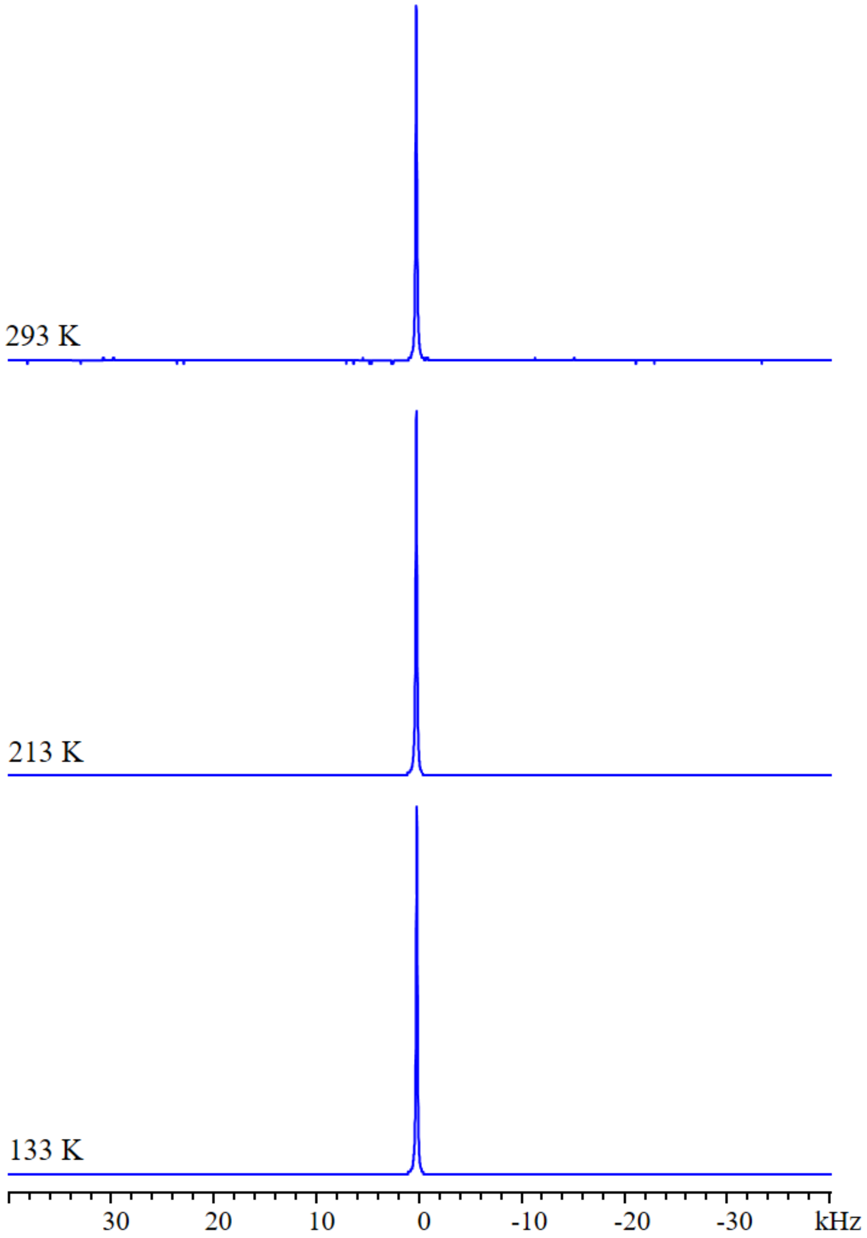

Figure S2. The experimental static variable-temperature ^{2}H SSNMR spectra of D_2 adsorbed within UiO-66 are shown. D_2 is highly mobile within the large cavities of UiO-66, giving rise to a sharp resonance at all experimental temperatures.

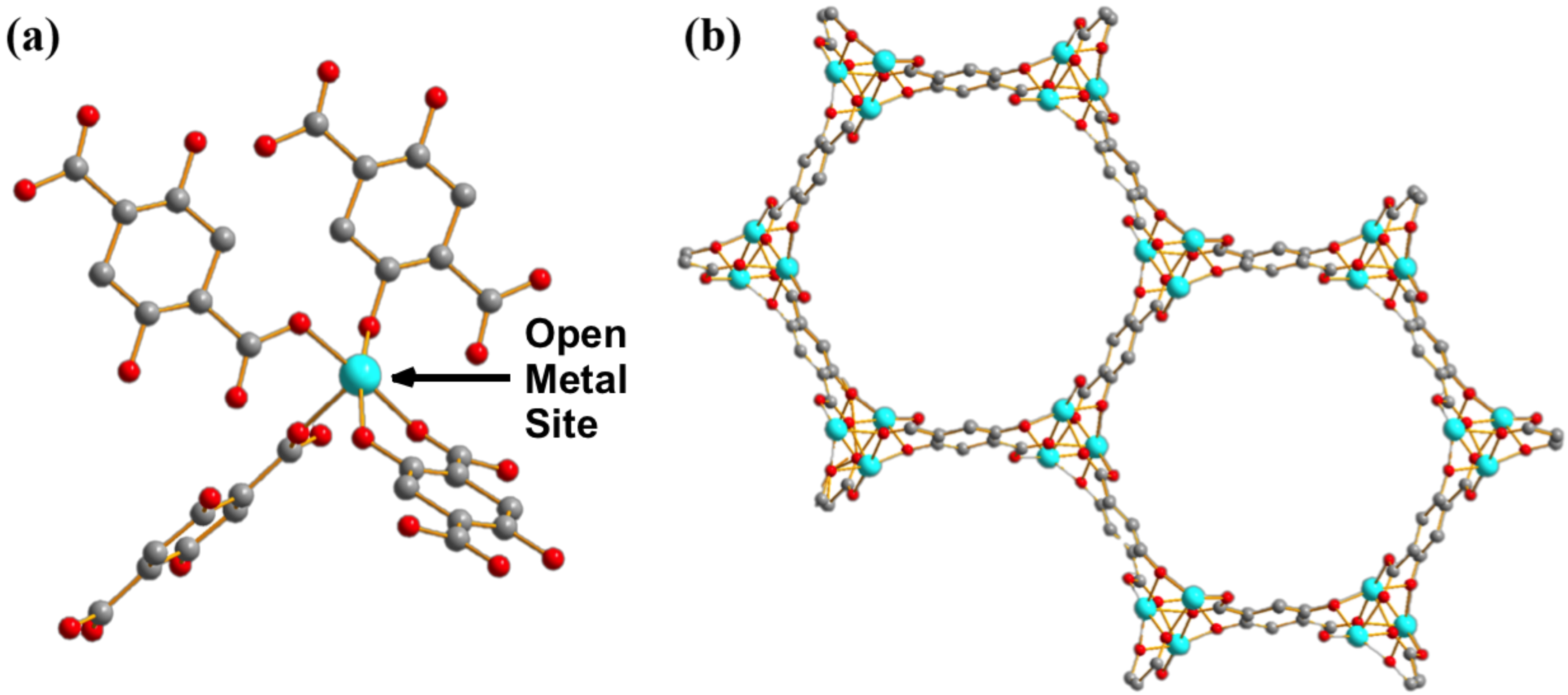

Figure S3. The local environment of the Mg center in activated MOF-74 is shown in (a), showing the coordinatively-unsaturated open metal site (OMS) accessible from the interior of the MOF channel. In (b), the one-dimensional honeycomb-shaped channels of MOF-74 are shown. The colors red, grey and cyan correspond to oxygen, carbon and the metal center, respectively. Hydrogen atoms are omitted for clarity.

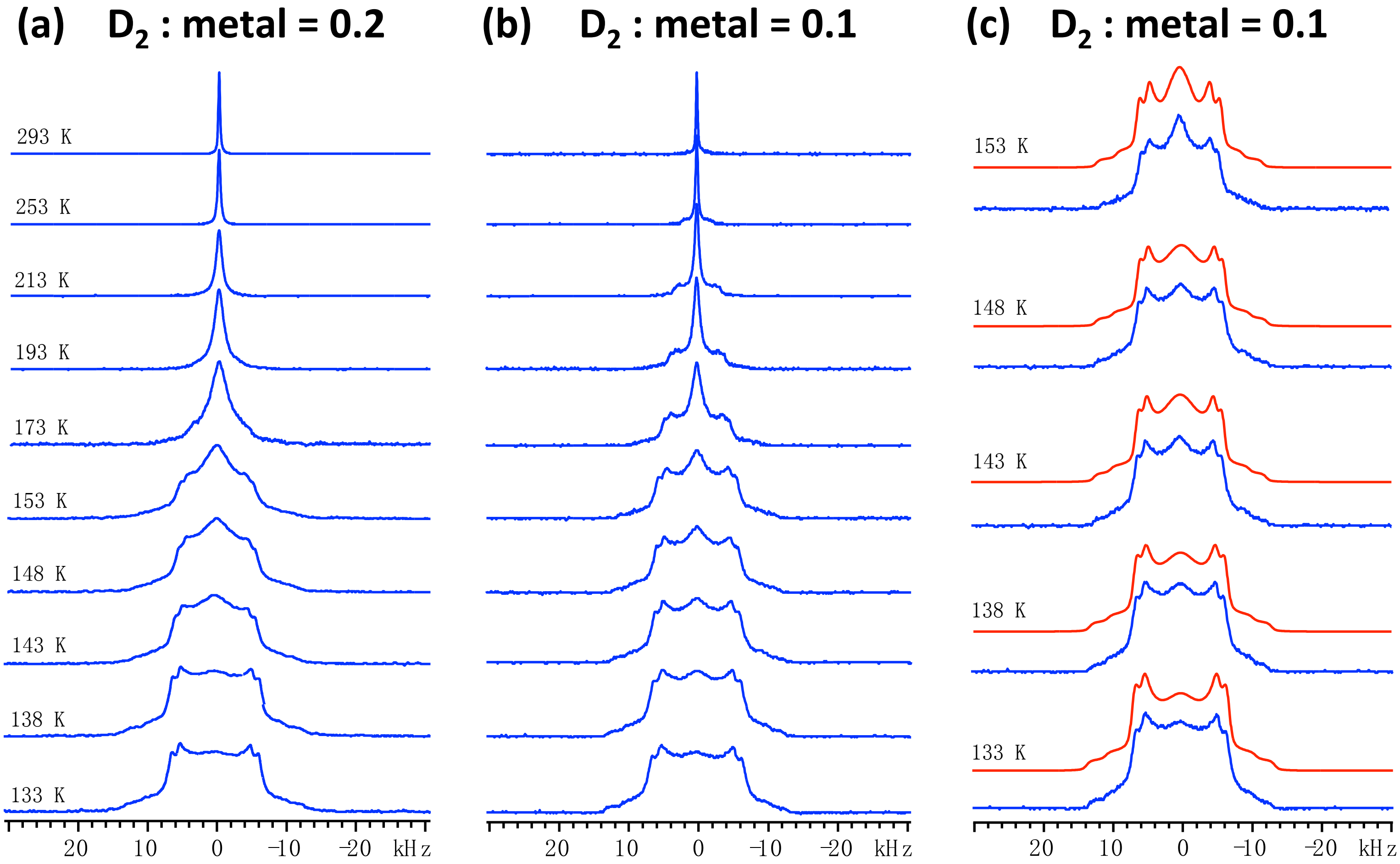

Figure S4. The experimental ^{2}H SSNMR spectra of D_2 loaded in Mg-MOF-74 at the loading levels of 0.2 and 0.1 D_2 : Mg are shown in (a) and (b), respectively. In (c), simulated spectra for the 0.1 loading level are shown, with corresponding parameters summarized in Table S2. See Figure S5 for a deconvolution of the 0.1 loading level simulations.

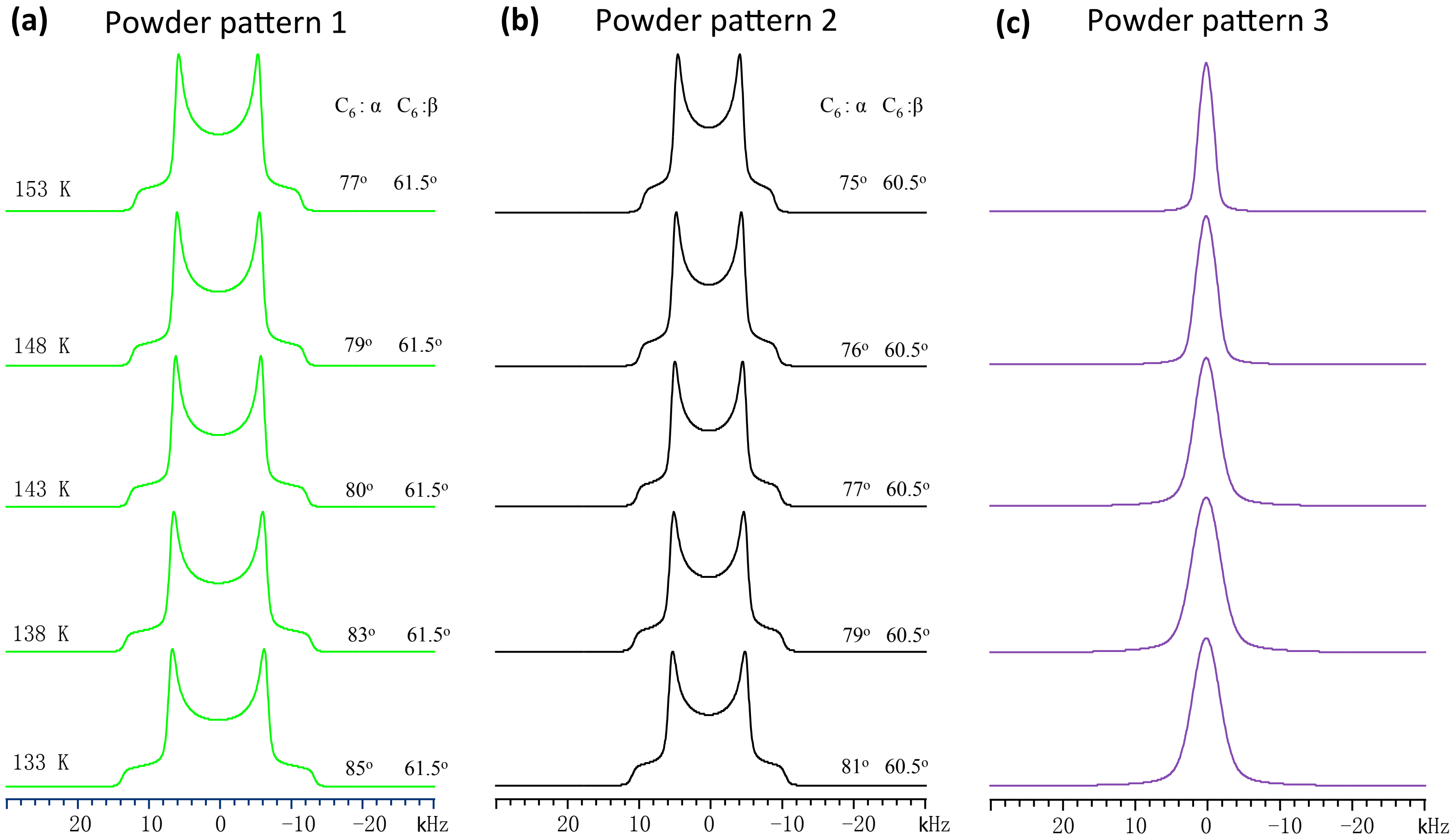

Figure S5. A deconvolution of the powder patterns that compose the ^{2}H SSNMR spectrum of 0.1 D_2/Mg loaded in Mg-MOF-74. The individual simulated spectra for each powder pattern are shown in (a), (b), and (c). All simulations were performed using the EXPRESS software[11] and a fast rate of motion (10^9 Hz). The C_6 sixfold rotation and accompanying angle α describe the localized wobbling of D_2 about the adsorption site (*i.e.*, open metal site), while the other C_6 motion and the angle β refer to a non-localized six-fold hopping of D_2 about the circumference of the MOF channel between open metal sites. The intensity ratio between powder patterns 1 and 2 is 1: 0.7 in this temperature range. Powder patterns 1 and 2 are assigned to D_2 adsorbed on the open metal site in slightly different geometries, orientations, and/or locations. The third powder pattern corresponds to free, mobile D_2 and is modeled by a narrow distribution.

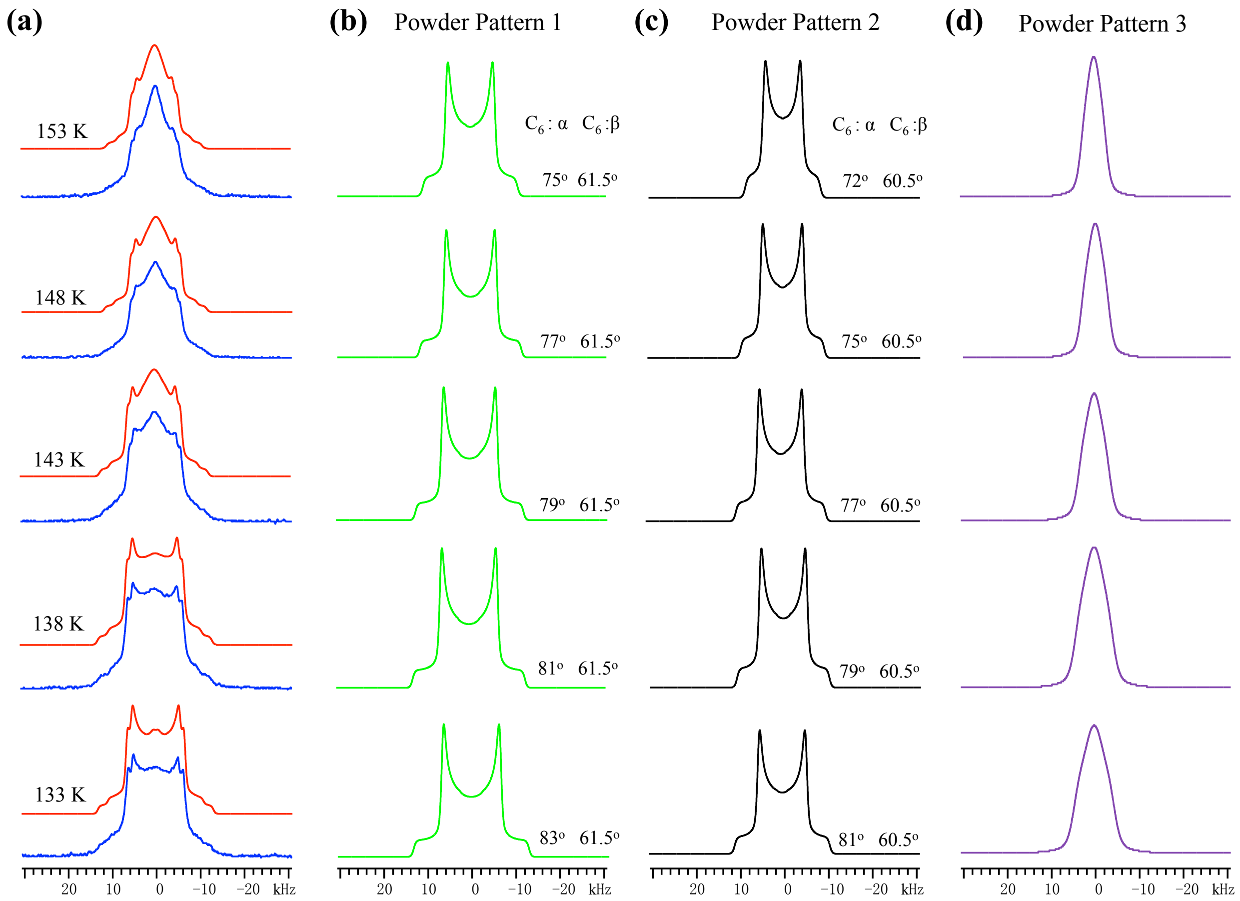

Figure S6. ^{2}H SSNMR spectra of D_2 adsorbed in Mg-MOF-74 at a loading level of 0.2 D_2 : Mg are illustrated. In (a), a comparison of experimental (blue) and simulated (red) static ^{2}H SSNMR spectra at low temperatures (from 153 K to 133 K) is shown. The individual simulated spectra for each powder pattern are shown in (b), (c), and (d). All simulations were performed using the EXPRESS software[11] and a fast rate of motion (10^9 Hz). The C_6 sixfold rotation and accompanying angle α describe the localized wobbling of D_2 at the adsorption sites on the open metal site, while the other C_6 motion and the angle β refer to a non-localized six-fold hopping about the circumference of the MOF channel between open metal sites. The intensity ratio between powder patterns 1 and 2 is 1: 0.7 in this temperature range. Powder patterns 1 and 2 are assigned to D_2 adsorbed on the open metal site, while powder pattern 3 corresponds to mobile D_2 not locally adsorbed to the MOF.

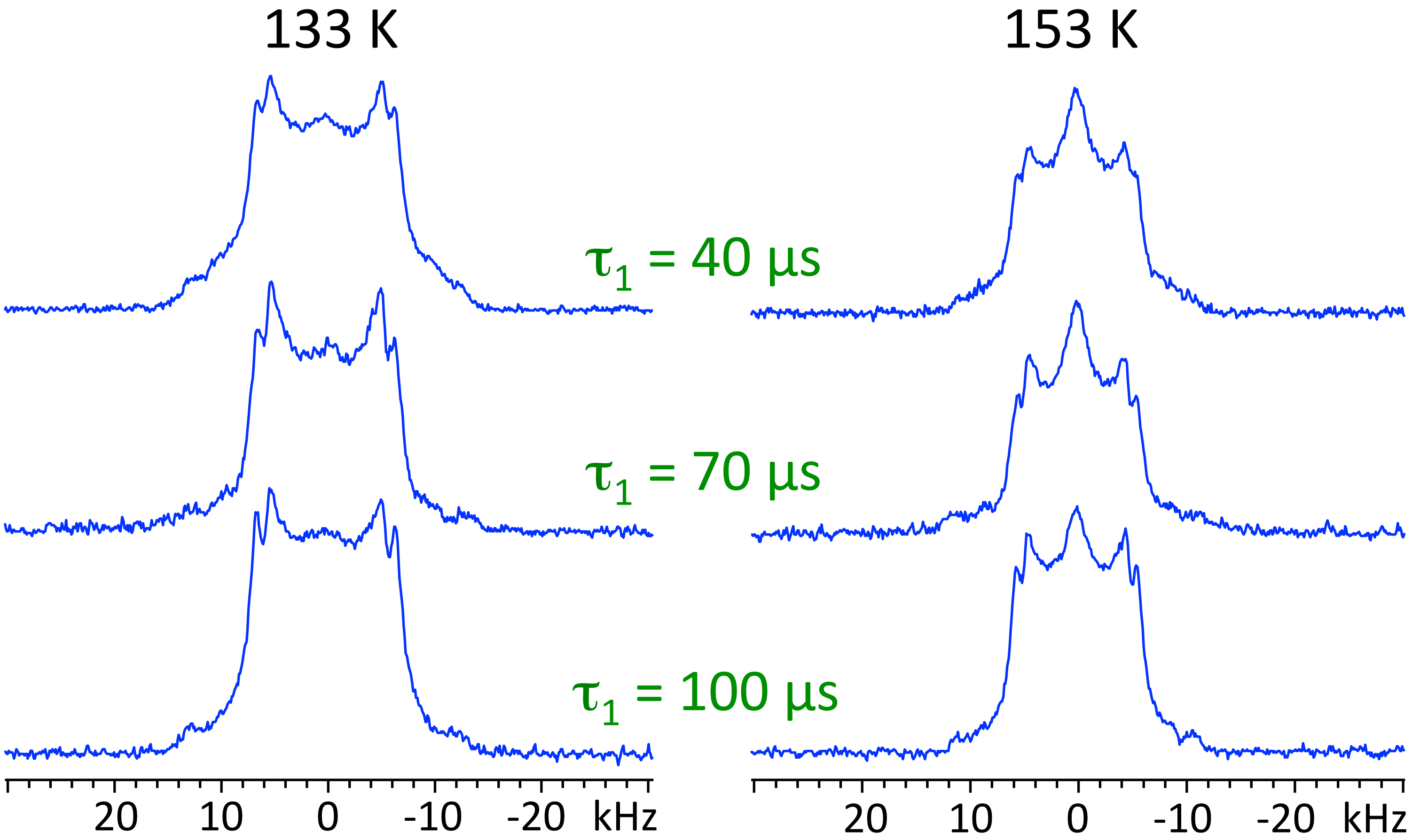

Figure S7. The ^{2}H SSNMR powder patterns of D_2 adsorbed in Mg-MOF-74 at 133 K (left column) and 153 K (right column), as obtained using different interpulse delays. The interpulse delay refers to the time period τ_1 between the two $\pi/2$ pulses in the solid-echo pulse sequence of the form $[(\pi/2) - \tau_1 - (\pi/2) - \tau_2$ – acquisition]. For both sets of experiments, a τ_2 value of 25 µs and a receiver delay of 20 µs were used. The lack of powder pattern variation at each temperature when the interpulse delay is varied confirms that both types of adsorbed D_2 molecules participate in dynamics at a rate located in the fast motion regime ($\geq 10^7$ Hz).

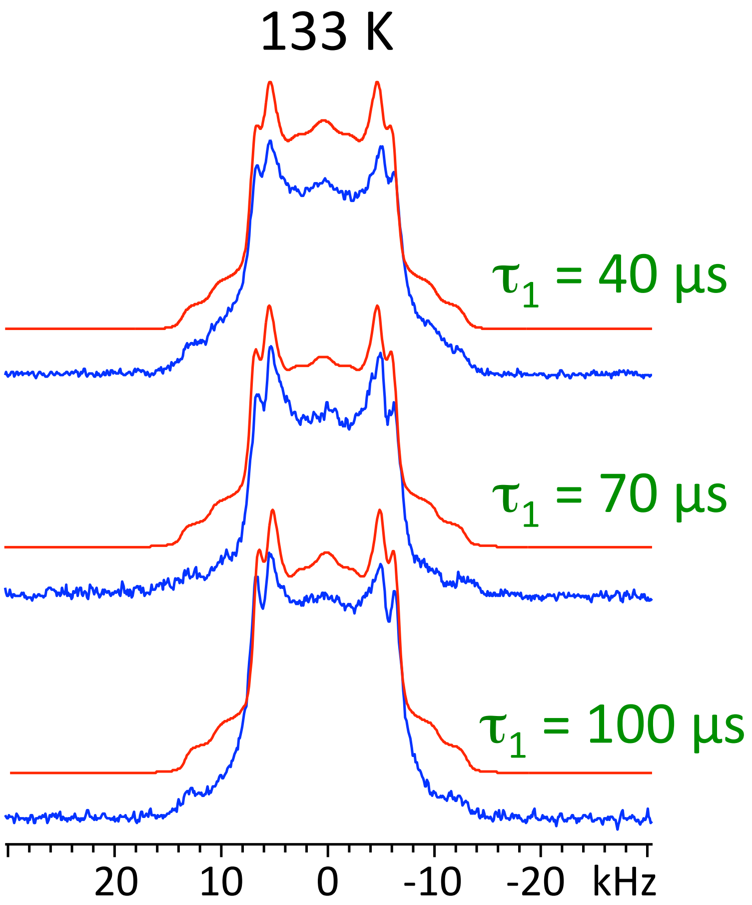

Figure S8. The simulated and experimental ^{2}H SSNMR spectra of D_2 adsorbed in Mg-MOF-74 at 133 K, as obtained using different interpulse delays. The interpulse delay refers to the time period τ_1 between the two $\pi/2$ pulses in the solid-echo pulse sequence of the form [$(\pi/2)$ - τ_1 - $(\pi/2)$ - τ_2 – acquisition]. A τ_2 value of 25 μs and a receiver delay of 20 μs were employed for the acquisition of all three spectra. The lack of powder pattern variation at each temperature when the interpulse delay is varied confirms that both types of adsorbed D_2 molecules are undergoing dynamics at a rate in the fast motion regime (≥ 10^7 Hz).

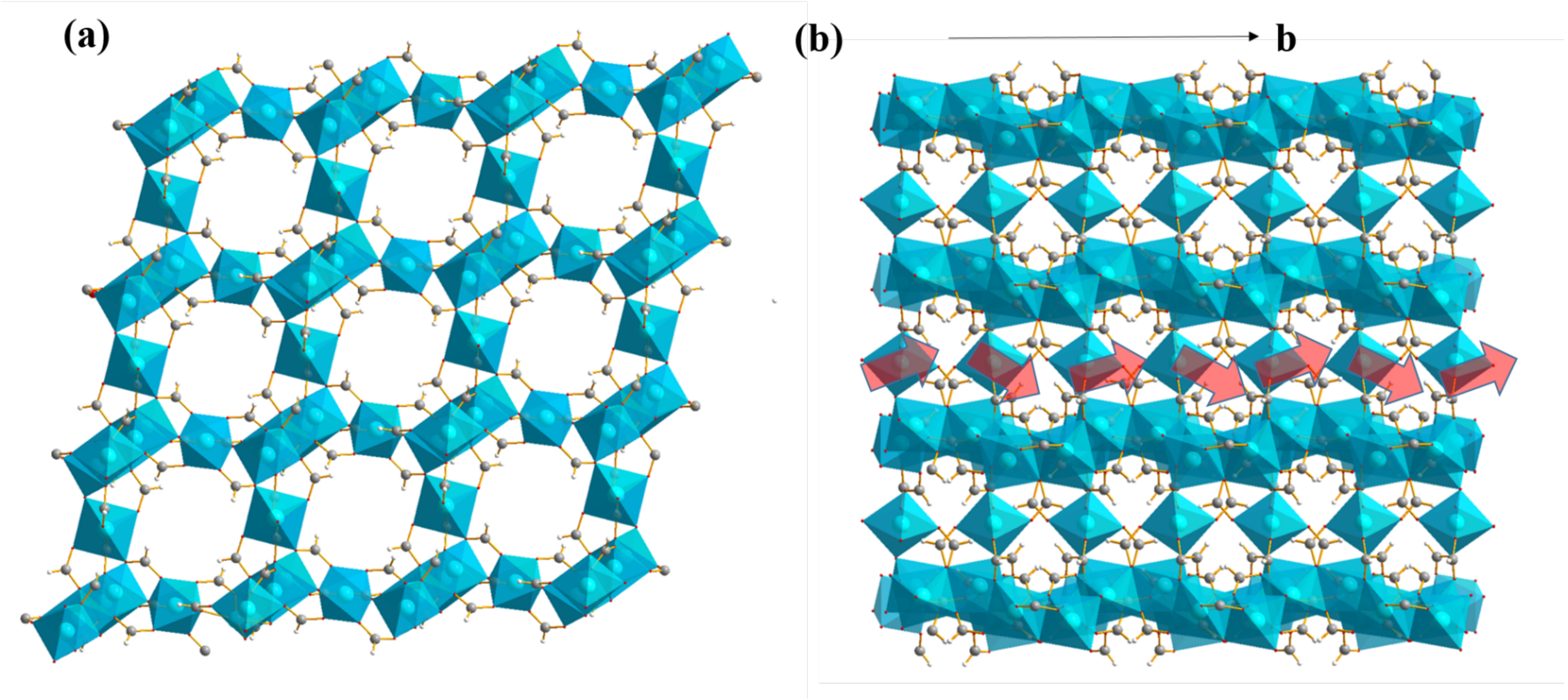

Figure S9. The structure of the α-$Mg_3(COOH)_6$ and α-$Zn_3(COOH)_6$ MOFs is shown, with views chosen to feature (a) the one-dimensional channels along the (0 1 0) direction, and (b) the zig-zag longitudinal shape of the channels along the crystallographic *b* axis.

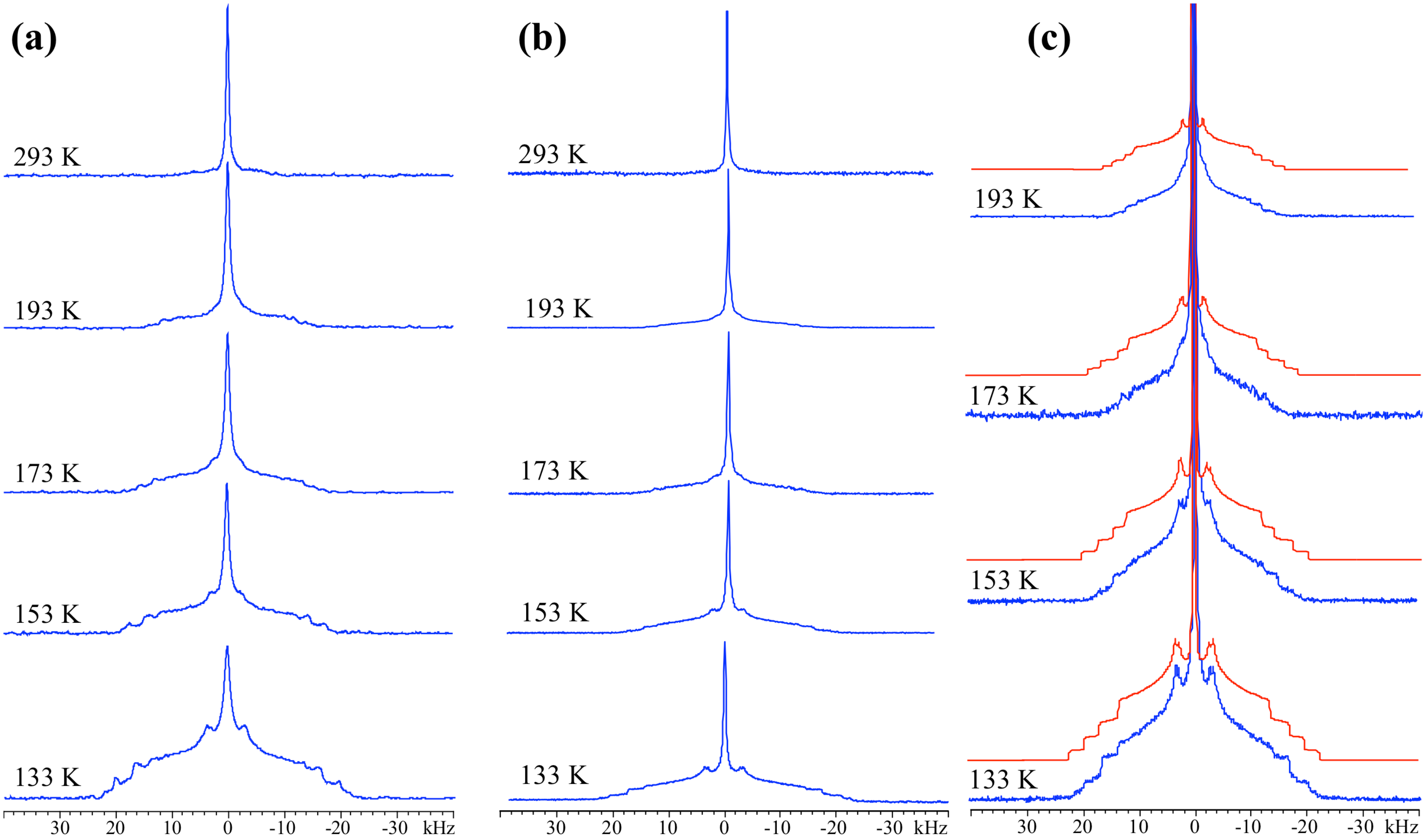

Figure S10. The experimental static variable-temperature ^{2}H SSNMR spectra of D_2 adsorbed within (a) α-$Mg_3(COOH)_6$ and (b) α-$Zn_3(COOH)_6$ are shown. In (c), both experimental (bottom blue trace) and simulated (top red trace) ^{2}H SSNMR spectra of D_2 in $Zn_3(COOH)_6$ at low temperatures are depicted, with the top of the intense central resonance truncated for clarity. See Tables S3 and S5 of the Supporting Information for tabulated NMR parameters and motional data. A preliminary simulation of the relatively more complicated α-$Mg_3(COOH)_6$ spectrum at 133 K is included in Supporting Information Figure S11.

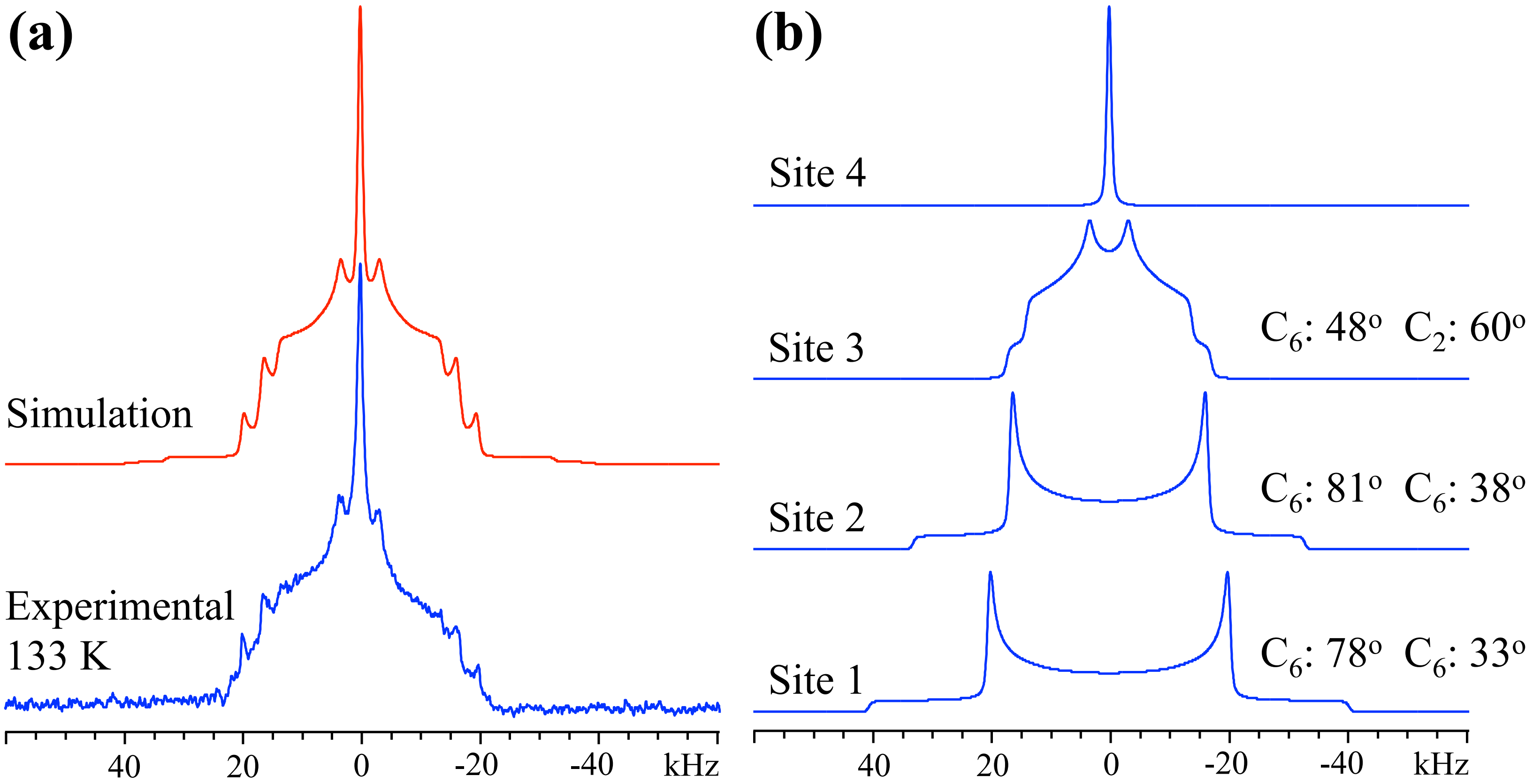

Figure S11. The experimental and simulated ^{2}H SSNMR spectra of D_2 adsorbed in α-$Mg_3(COOH)_6$ are shown in (a), while a deconvolution of the simulation showing three powder patterns of adsorbed D_2 and a narrow fourth resonance corresponding to mobile D_2 are shown in (b). The first listed motional angle in (b) is for a localized sixfold rotation or "wobbling," while the second is for a non-localized twofold hopping (site 3) or a sixfold hopping (sites 1 and 2) of D_2 molecules. This simulation should be treated as preliminary for the purposes of dynamic information, however, the presence of three main H_2 adsorption sites in α-$Mg_3(COOH)_6$ strongly agrees with a very recent report.[12] The powder pattern shapes and extracted motional information imply that adsorption sites 1 and 2 are in similar environments, while adsorption site 3 is in a distinct environment.

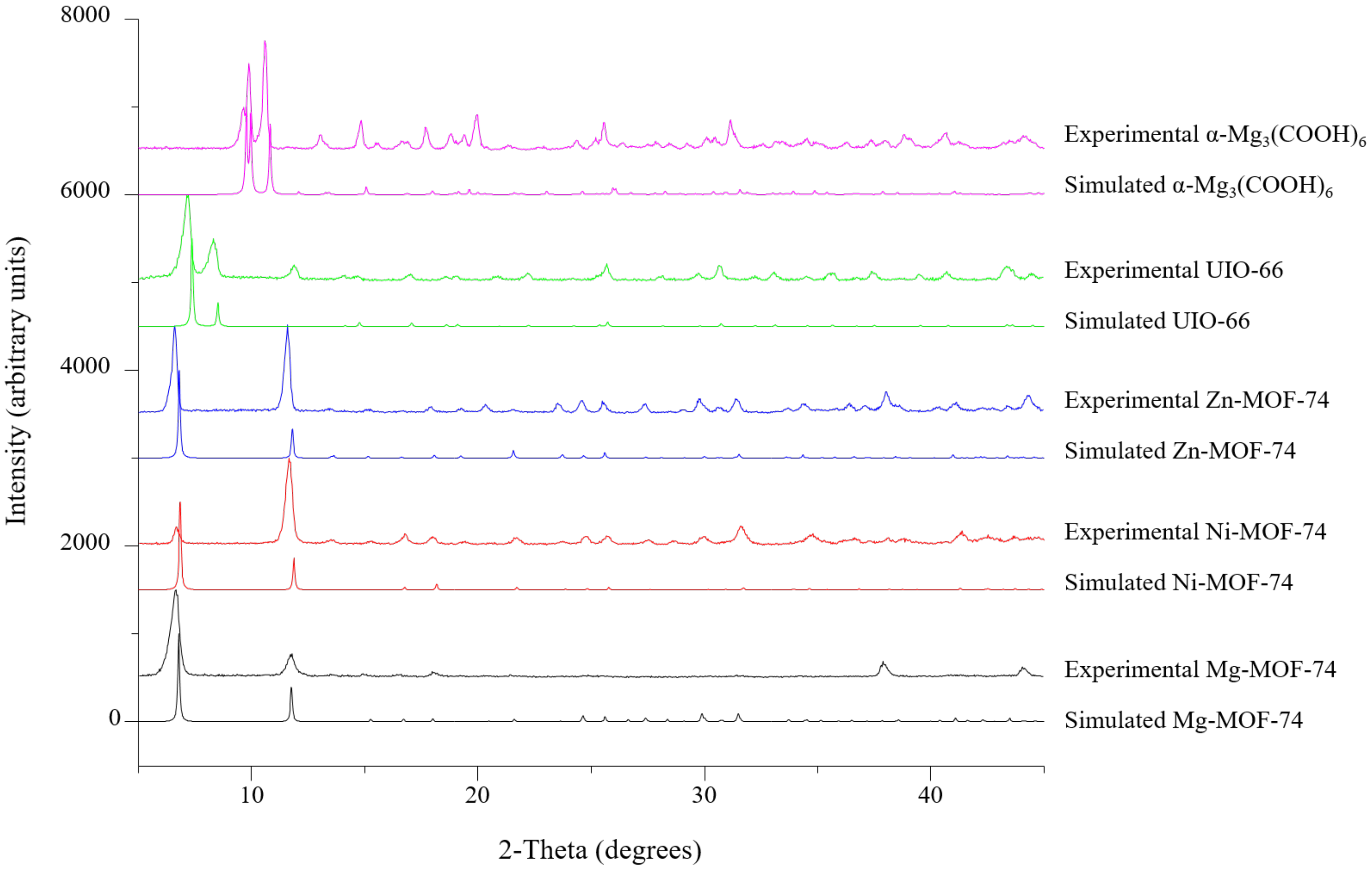

Figure S12. The experimental and simulated powder X-ray diffraction patterns of the MOFs included in this study.

Table S1. The observed ^{2}H quadrupolar parameters in D_2-loaded Mg-MOF-74 at a loading level of 0.2 D_2/metal.[a,b,c]

Temperature (K)	Site	Relative intensity	C_Q (kHz)	η_Q
153	1	1	14.3(1)	0
	2	0.7	11.2(1)	0
148	1	1	15.3(1)	0
	2	0.7	12.4(1)	0
143	1	1	16.2(1)	0
	2	0.7	13.3(1)	0
138	1	1	17.0(2)	0
	2	0.7	13.9(1)	0
133	1	1	17.3(2)	0
	2	0.7	14.3(1)	0

[a] The loading level of D_2:Mg was 0.2 in this sample of Mg-MOF-74, see Experimental details in Supporting Information. See Table S2 for NMR parameters of a 0.1 D_2:Mg sample. [b] The numbers in the parentheses correspond to the uncertainties in experimental parameters. [c] In these simulations, a sharp isotropic resonance at ca. 0 ppm was used to simulate the narrow, intense signal corresponding to mobile D_2, which lacks any quadrupolar parameters.

Table S2. The observed ^{2}H quadrupolar parameters in D_2-loaded Mg-MOF-74 at a loading level of 0.1 D_2/metal.[a,b,c]

Temperature (K)	Site	Relative intensity	C_Q (kHz)	η_Q
153	1	1	15.6(1)	0
	2	0.7	12.3(1)	0
148	1	1	16.2(1)	0
	2	0.7	12.9(1)	0
143	1	1	16.7(1)	0
	2	0.7	13.4(1)	0
138	1	1	17.5(2)	0
	2	0.7	13.9(1)	0
133	1	1	18.9(2)	0
	2	0.7	14.3(1)	0

[a] The loading level of D_2:Mg was 0.1 in this sample of Mg-MOF-74, see Experimental details in Supporting Information. [b] The numbers in the parentheses correspond to the uncertainties in experimental parameters. [c] In these simulations, a sharp isotropic resonance at ca. 0 ppm was used to simulate the narrow, intense signal corresponding to mobile D_2, which lacks any quadrupolar parameters.

Table S3. The dynamic information of D_2 guests in the Mg-MOF-74 and α-$Zn_3(COOH)_6$ MOFs.[a]

Compound	Temperature (° K)	Site	Wobbling angle (°)	Hopping angle (°)
Mg-MOF-74	153	1	75(2)	61.5(20)
		2	72(2)	60.5(20)
	148	1	77(2)	61.5(20)
		2	75(2)	60.5(20)
	143	1	79(1)	61.5(10)
		2	77(1)	60.5(10)
	138	1	81(1)	61.5(10)
		2	79(1)	60.5(10)
	133	1	83(1)	61.5(10)
		2	81(1)	60.5(10)
α-$Zn_3(COOH)_6$	193	1	47(2)	38(2)
		2	44.5(20)	37.5(20)
	173	1	46.5(20)	38(2)
		2	42.5(20)	37.5(20)
	153	1	45.5(10)	38.5(10)
		2	41.5(10)	38(1)
	133	1	46(1)	39.5(10)
		2	40(1)	37.5(10)

[a] The rate of D_2 motion was in the fast regime (i.e., ≥ 10^9 Hz) throughout the experimental temperature range for both systems. For Mg-MOF-74, both the localized rotational "wobbling" and non-localized hopping motions of D_2 are sixfold (i.e., C_6). In α-$Zn_3(COOH)_6$, the wobbling motion of D_2 was modeled by a sixfold (C_6) rotation, while the hopping motion was twofold (C_2).

Table S4. The observed ^{2}H quadrupolar parameters in D_2-loaded Mg-MOF-74 at a temperature of 133 K and a loading level of 0.1 D_2/metal, as a function of changes in the interpulse delay.[a,b,c]

Interpulse delay (μs)	Site	Relative intensity	C_Q (kHz)	η_Q
40	1	1	18.9(2)	0
	2	0.70(3)	14.3(1)	0
70	1	1	18.9(2)	0
	2	0.72(3)	14.3(1)	0
100	1	1	18.9(2)	0
	2	0.65(4)	14.3(1)	0

[a] The interpulse delay refers to the time period τ_1 between the two $\pi/2$ pulses in the solid-echo pulse sequence of the form $[(\pi/2) - \tau_1 - (\pi/2) - \tau_2 -$ acquisition] . [b] The numbers in the parentheses correspond to the uncertainties in experimental parameters. [c] In these simulations, a sharp isotropic resonance at ca. 0 ppm was used to simulate the narrow, intense signal corresponding to mobile D_2, which lacks any quadrupolar parameters.

Table S5. The observed ^{2}H quadrupolar parameters in D_2-loaded α-$Zn_3(COOH)_6$.[a,b,c]

Temperature (K)	**Site**[c]	**Relative intensity**	C_Q **(kHz)**	η_Q
193	1	1	17.0(2)	0.72(2)
	2	1	22.5(2)	0.77(3)
173	1	1	18.3(4)	0.73(2)
	2	0.78	25.0(2)	0.76(3)
153	1	0.94	20.0(4)	0.69(3)
	2	1	28.0(4)	0.73(2)
133	1	1	23.5(5)	0.60(3)
	2	1	31.0(3)	0.76(2)

[a] The loading level of D_2 : Zn was 0.1 in this sample of α-$Zn_3(COOH)_6$. [b] The numbers in the parentheses correspond to the uncertainties in experimental parameters. [c] In these simulations, a sharp isotropic resonance at ca. 0 ppm was used to simulate the narrow, intense signal corresponding to mobile D_2, which lacks any quadrupolar parameters.

Appendix A: Justification of two D_2 adsorption sites in Mg-MOF-74

We would like to begin by clarifying that the ^{2}H SSNMR spectra of Mg-MOF-74 exhibit 3 independent resonances, however, the narrow central resonance corresponds to free D_2 that is not locally adsorbed within MOF-74. To avoid any confusion, we accurately modeled this central narrow resonance using a mix of Gaussian and Lorentzian distributions, rather than NMR parameters. The observation of free D_2 is logical at these relatively high temperatures and occurs in other MOFs within this study, such as α-$Mg_3(COOH)_6$ and α-$Zn_3(COOH)_6$. With this in mind, we are only concerned with the two separate broad ^{2}H powder patterns associated with adsorbed D_2. These powder patterns corresponding to two unique D_2 adsorption sites within Mg-MOF-74, which are proximate to each other and both located on the OMS (*vide infra*).

We have embarked on a thorough examination of the literature, which revealed that two reports have both postulated the possible presence of two very similar D_2 binding sites in the MOF-74 family at loading levels similar to those used in this study on the basis of infrared spectroscopy and inelastic neutron scattering.[13, 14] These two adsorption sites are hypothesized to be very similar in adsorption enthalpy and location.[14] The literature is unanimous that H_2/D_2 is only adsorbed on the OMSs at this loading level, and that no other adsorption locations are populated.[15, 16] Furthermore, owing to the low D_2:Mg loading levels of 0.2 and 0.1 employed in this study, we can safely assume that no two D_2 molecules are adsorbed on the same OMS at any time.

We have explored the possibility of a single D_2 exchange between multiple sites in the intermediate dynamics regime. We have exhaustively attempted to fit our spectra using a single D_2 exchange between multiple sites, employing many different combinations of motional types, rates, and angles, including contributions in the intermediate and slow motion regimes. A key detail to note is the characteristic two sets of "horns" in these ^2H SSNMR spectra cannot be reproduced by any one-site simulation that attempts to fit the powder pattern. It is exceedingly clear from this information that there is no combination of motion that can fit this spectrum using a single D_2 exchange; the only possible fit for our experimental data that is consistent across the temperature range is a combination of sixfold non-localized hopping and a localized rotation or "wobbling" (modeled by a C_3, C_4, C_5, or C_6 rotation) at two distinct but similar adsorption sites. If there were indeed exchange between these two types of adsorbed D_2, we would expect to observe a single ^2H powder pattern, which we do not.

The following Figures in this Appendix show some of our many attempts to fit the ^2H SSNMR spectra using a single D_2 adsorption site and several different types of motions. As can be seen, it is impossible to recreate the characteristic double "horns" and distinct "shoulders" of the low-temperature spectra using a single adsorption site.

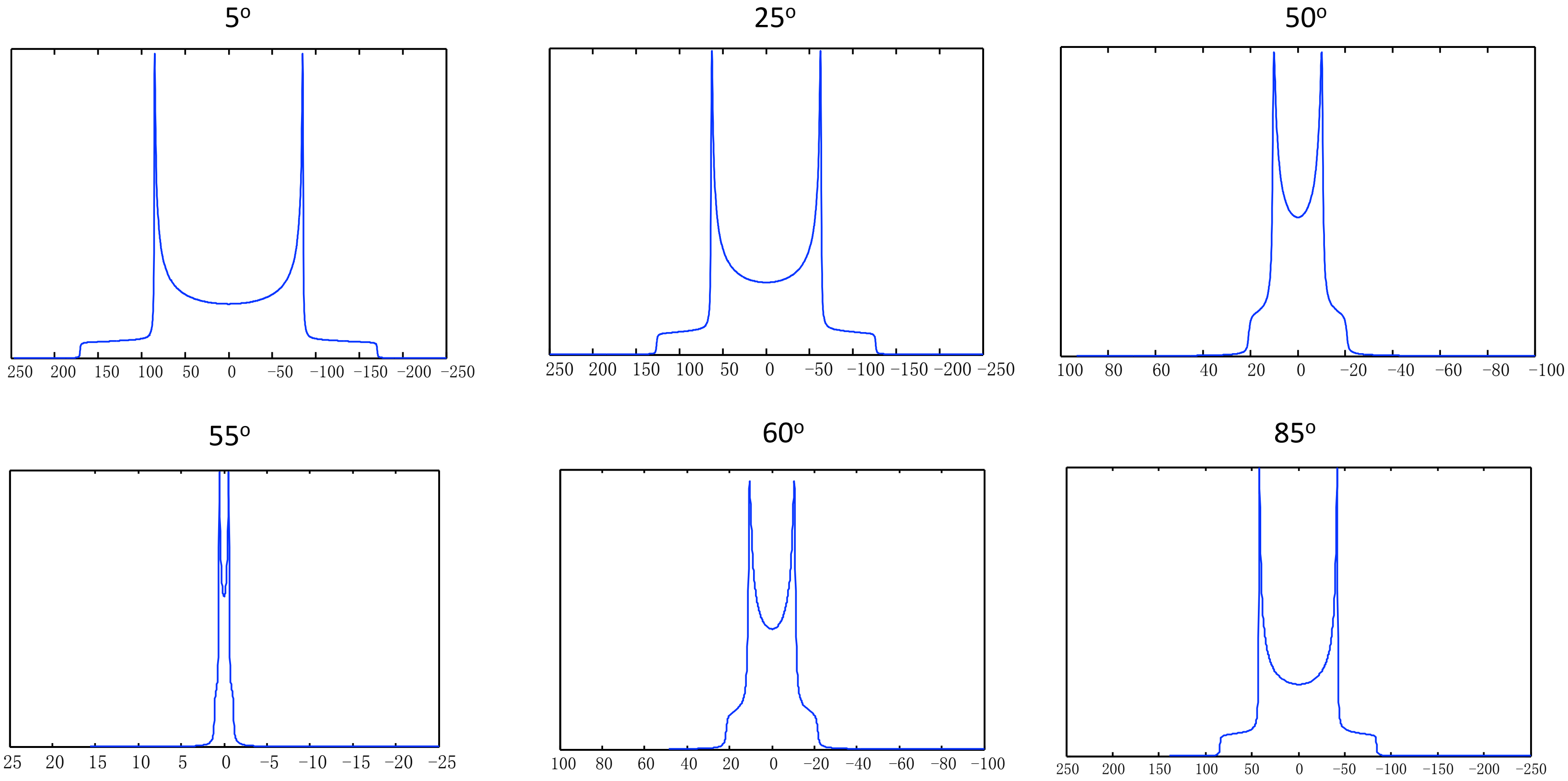

Figure A1. 1-site ^{2}H NMR dynamic simulations, assuming only a C_6 rotation (wobbling) of D_2 in Mg-MOF-74 with a rate 5 x 10^9 Hz (*i.e.*, in the fast motion regime). The rotation angle is indicated above each simulation. The horizontal axis is labeled in kHz.

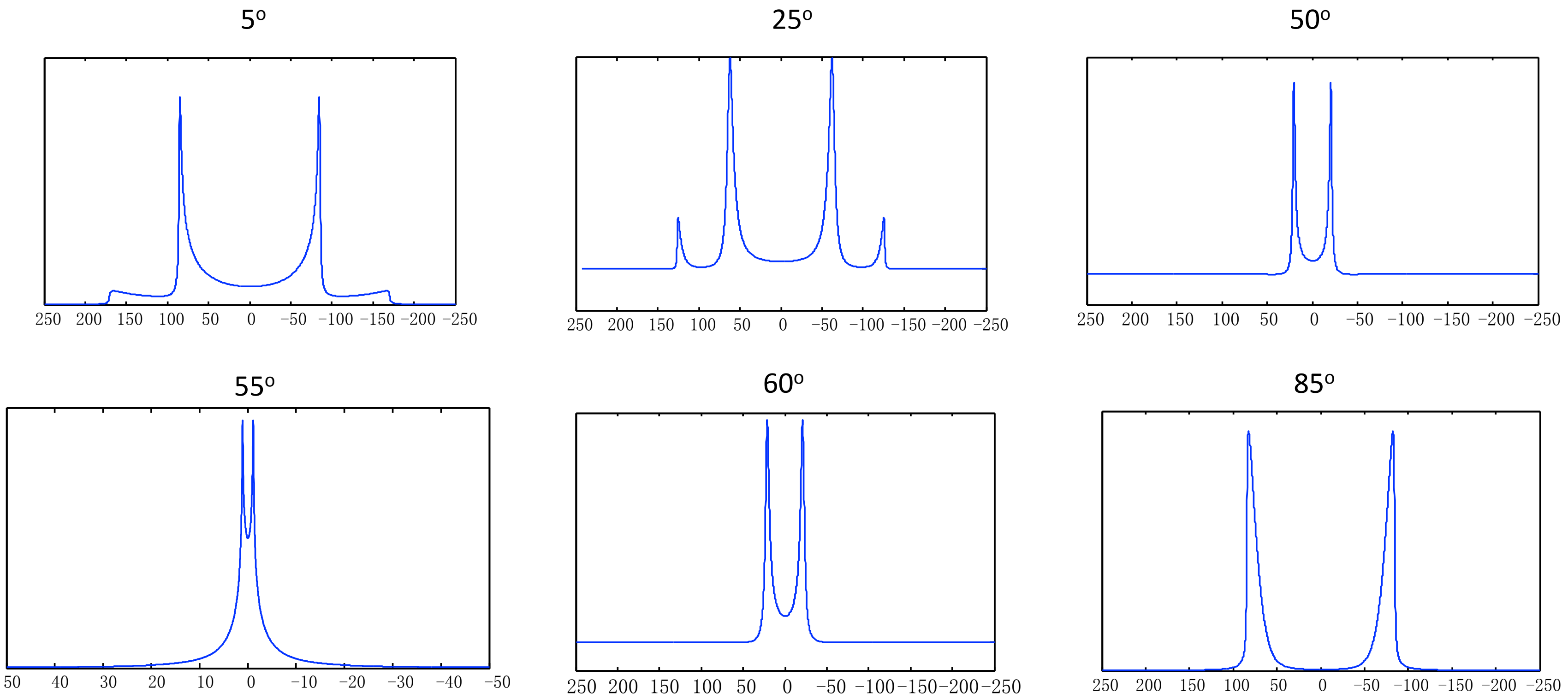

Figure A2. 1-site ^{2}H NMR dynamic simulations, assuming only a C_6 rotation (wobbling) of D_2 in Mg-MOF-74 with a rate 5 x 10^6 Hz (*i.e.*, in the intermediate motion regime). The rotation angle is indicated above each simulation. The horizontal axis is labeled in kHz.

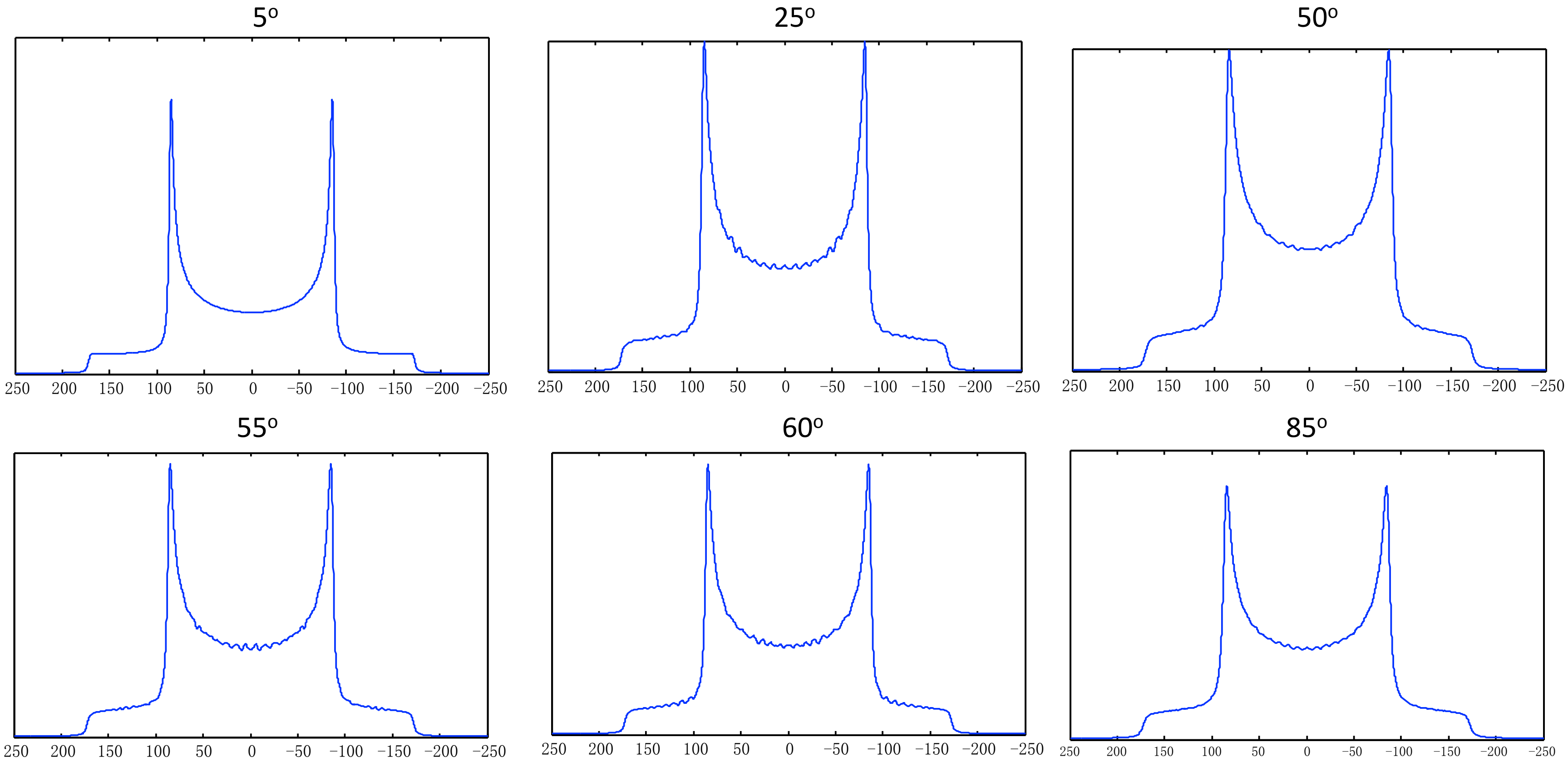

Figure A3. 1-site ^{2}H NMR dynamic simulations, assuming only a C_6 rotation (wobbling) of D_2 in Mg-MOF-74 with a rate 5 x 10^3 Hz (*i.e.*, in the slow motion regime). The rotation angle is indicated above each simulation. The horizontal axis is labeled in kHz.

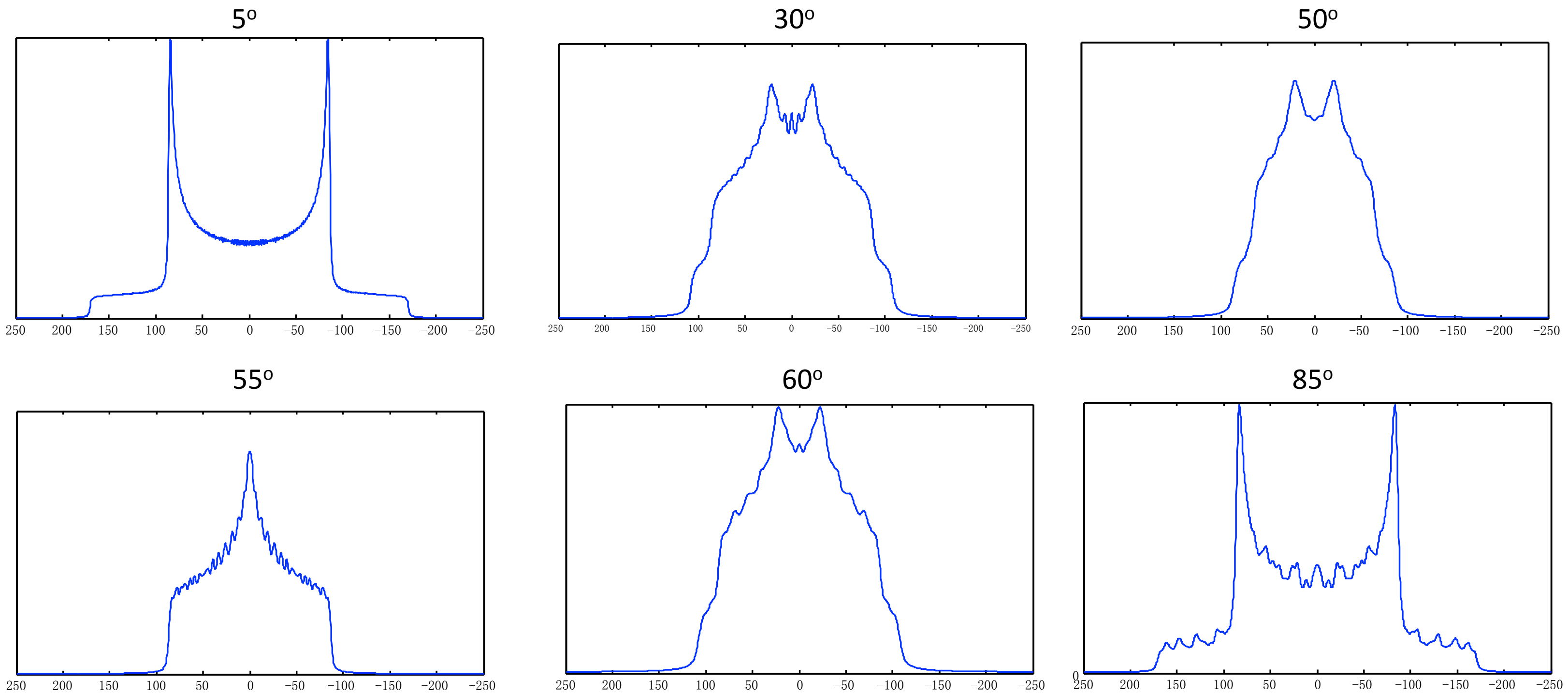

Figure A4. 1-site ^{2}H NMR dynamic simulations, assuming only a C_2 rotation (hopping) of D_2 in Mg-MOF-74 with a rate 5 x 10^9 Hz (*i.e.*, in the fast motion regime). The rotation angle is indicated above each simulation. The horizontal axis is labeled in kHz.

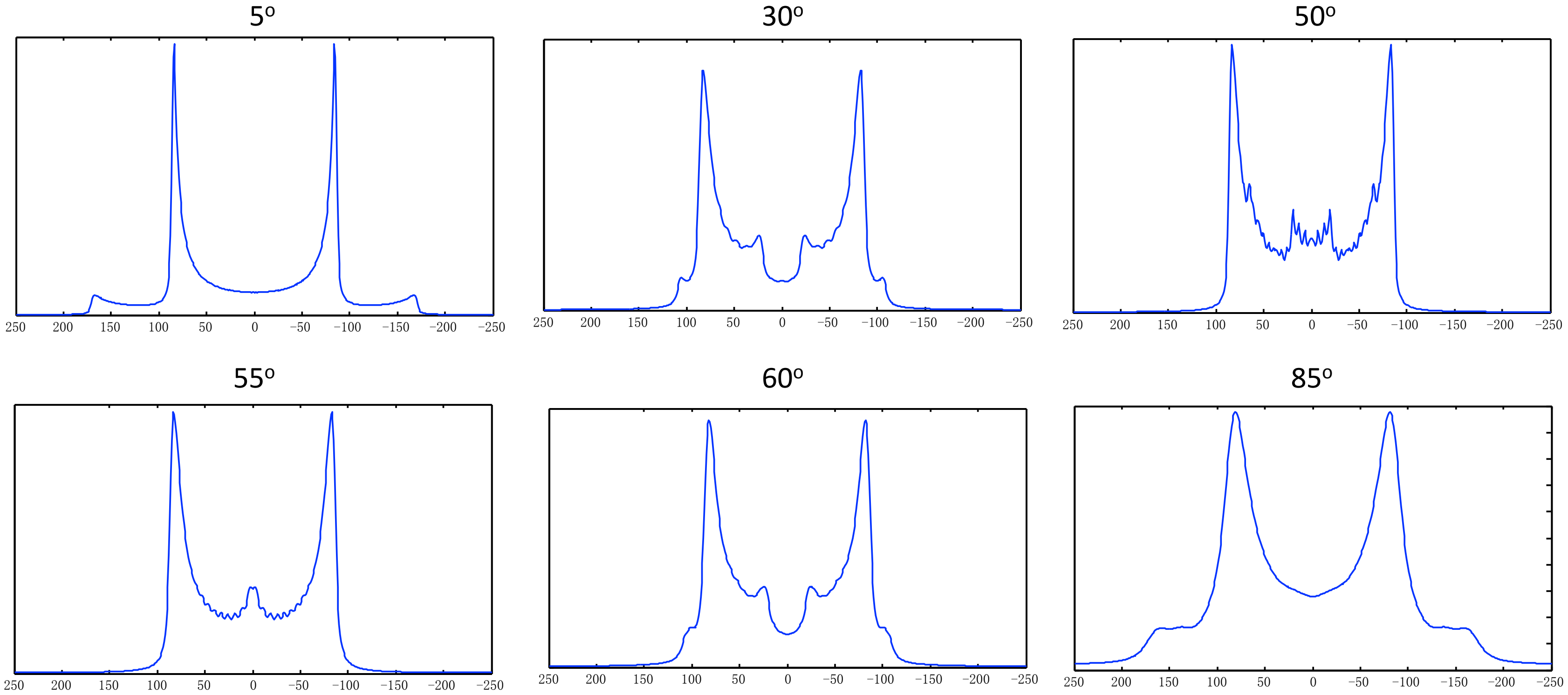

5º

30º

50º

55º

60º

85º

Figure A5. 1-site ^{2}H NMR dynamic simulations, assuming only a C_2 rotation (hopping) of D_2 in Mg-MOF-74 with a rate 5 x 10^{6} Hz (*i.e.*, in the intermediate motion regime). The rotation angle is indicated above each simulation. The horizontal axis is labeled in kHz.

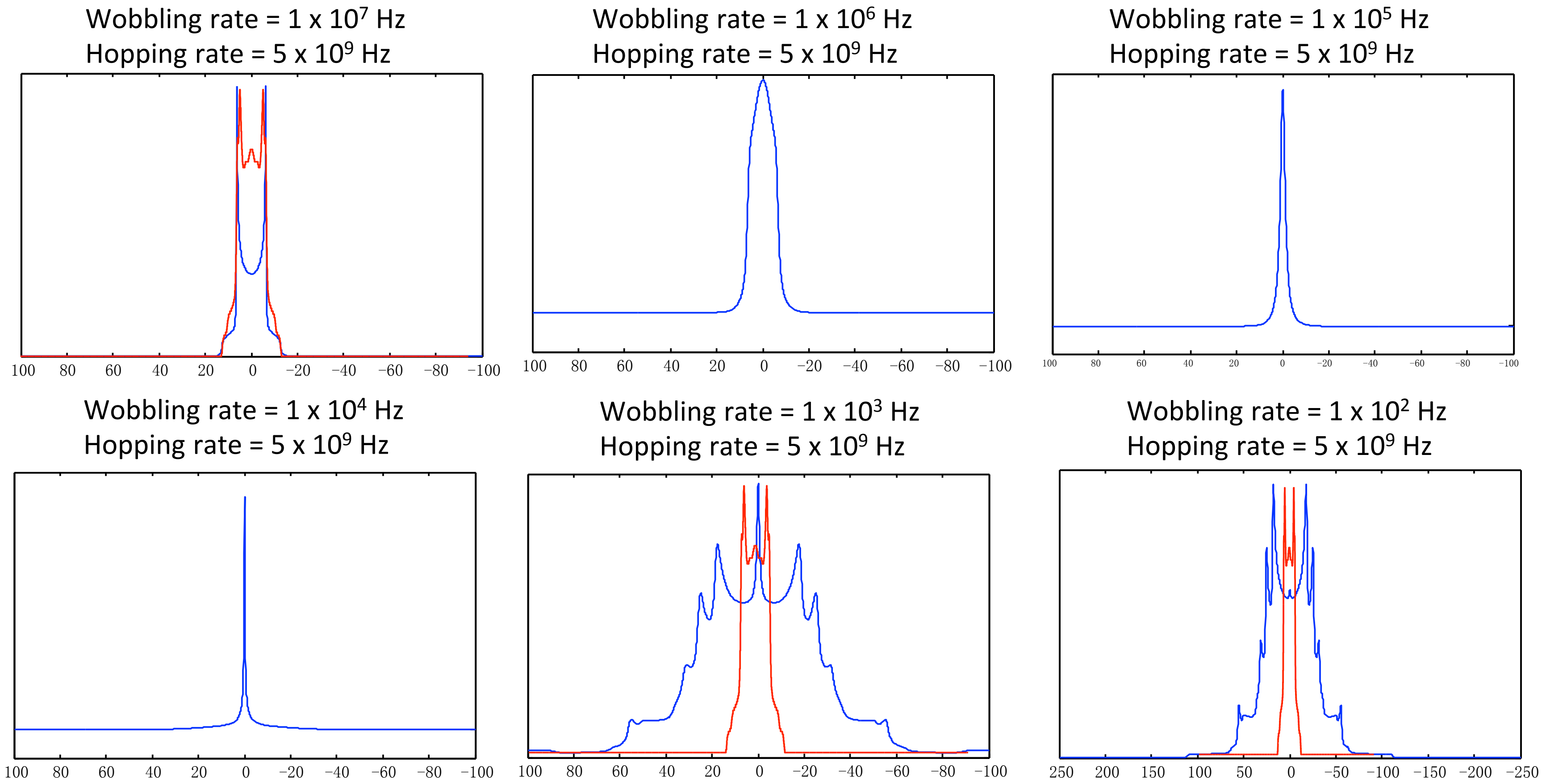

Figure A6. 1-site ^{2}H NMR dynamic simulations, assuming a C_6 rotation (wobbing through an angle α = 83^o) and another C_6 rotation (hopping through an angle β = 61.5^o) of D_2 in Mg-MOF-74. Different wobbling rates are explored while holding the hopping rate constant at 5 x 10^9 Hz (*i.e.*, in the fast motion regime). The horizontal axis is labeled in kHz. Experimental spectra are indicated in red for any simulations that resemble the lineshape. ***Note the positions and characteristic splitting of the spectral horns are not reproduced by the simulation at top left, nor are the positions of the outer spectral "shoulders," despite other similarities.***

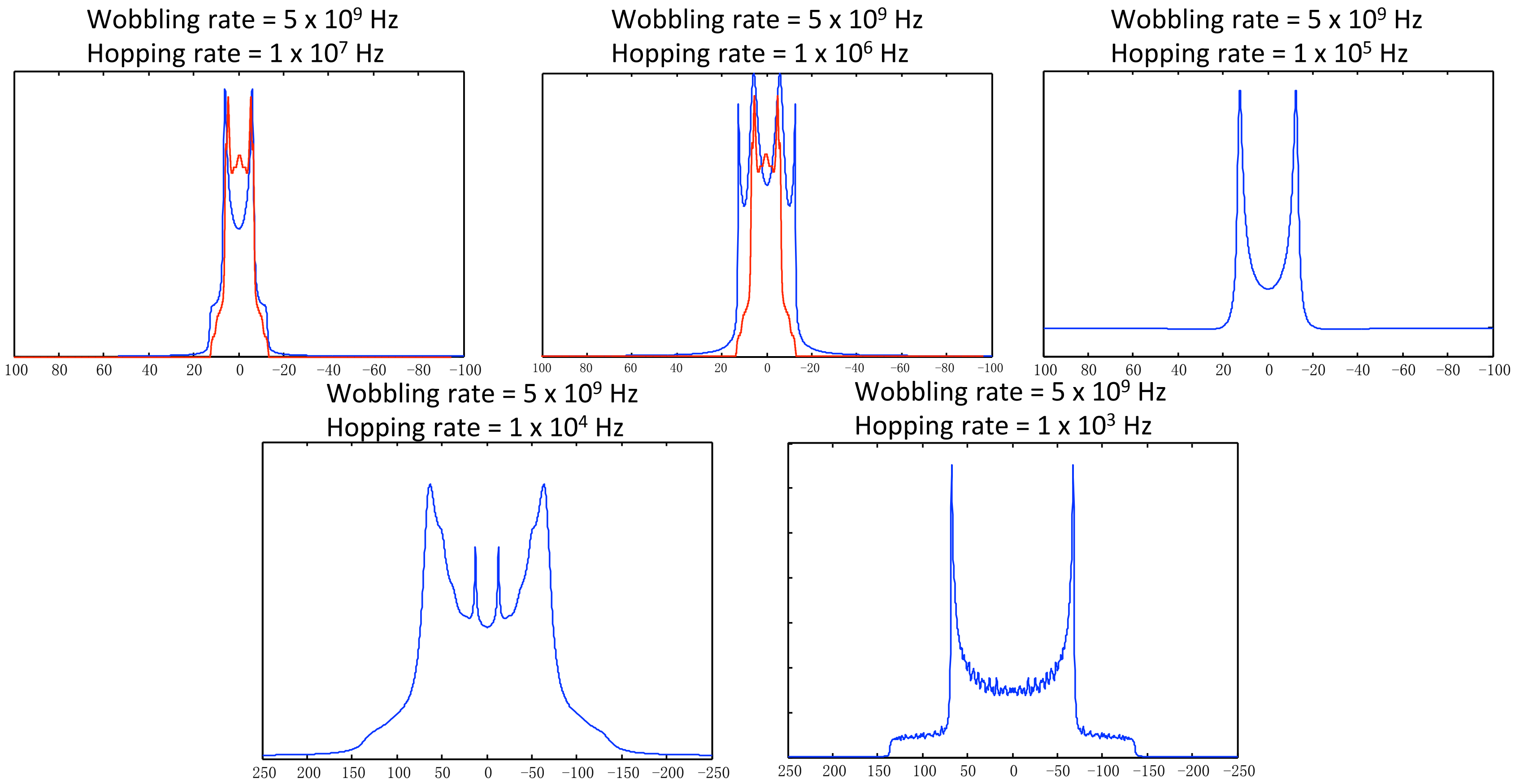
Wobbling rate = 5 x 10^9 Hz
Hopping rate = 1 x 10^7 Hz

Wobbling rate = 5 x 10^9 Hz
Hopping rate = 1 x 10^6 Hz

Wobbling rate = 5 x 10^9 Hz
Hopping rate = 1 x 10^5 Hz

Wobbling rate = 5 x 10^9 Hz
Hopping rate = 1 x 10^4 Hz

Wobbling rate = 5 x 10^9 Hz
Hopping rate = 1 x 10^3 Hz

Figure A7. 1-site ^{2}H NMR dynamic simulations, assuming a C_6 rotation (wobbing through an angle $\alpha = 83^{o}$) and another C_6 rotation (hopping through an angle $\beta = 61.5^{o}$) of D_2 in Mg-MOF-74. Different hopping rates are explored while holding the wobbling rate constant at 5 x 10^9 Hz (*i.e.*, in the fast motion regime). The horizontal axis is labeled in kHz. Experimental spectra are indicated in red for any simulations that resemble the lineshape. ***Note the positions and characteristic splitting of the spectral horns are not reproduced by the simulation at top left, nor are the positions of the outer spectral "shoulders," despite other similarities.***

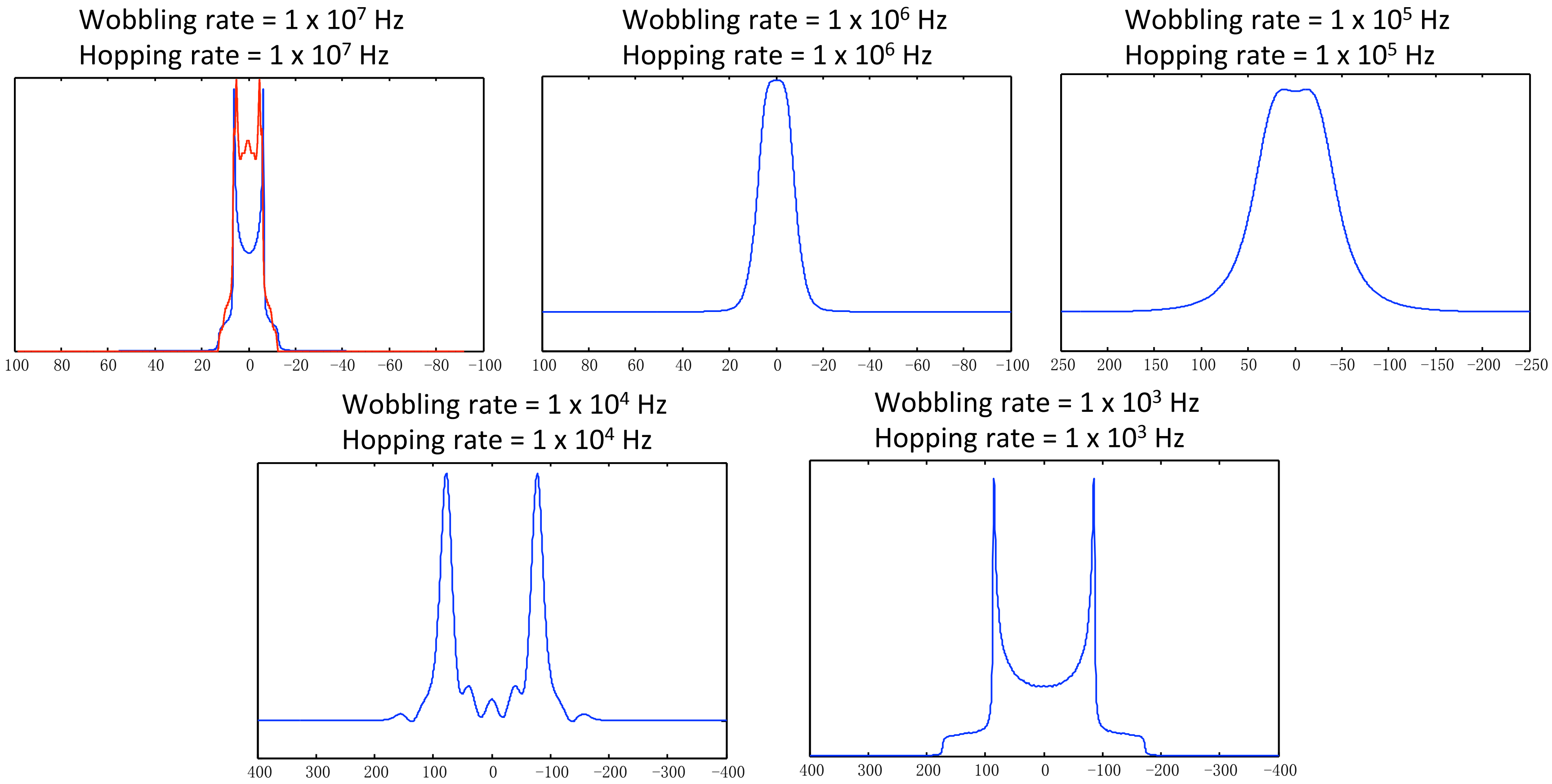

Wobbling rate = 1 x 10^7 Hz
Hopping rate = 1 x 10^7 Hz

Wobbling rate = 1 x 10^6 Hz
Hopping rate = 1 x 10^6 Hz

Wobbling rate = 1 x 10^5 Hz
Hopping rate = 1 x 10^5 Hz

Wobbling rate = 1 x 10^4 Hz
Hopping rate = 1 x 10^4 Hz

Wobbling rate = 1 x 10^3 Hz
Hopping rate = 1 x 10^3 Hz

Figure A8. 1-site ^{2}H NMR dynamic simulations, assuming a C_6 rotation (wobbing through an angle α = 83^o) and another C_6 rotation (hopping through an angle β = 61.5^o) of D_2 in Mg-MOF-74. Different hopping and wobbling rates are simultaneously explored. The horizontal axis is labeled in kHz. Experimental spectra are indicated in red for any simulations that resemble the lineshape. ***Note the positions and characteristic splitting of the spectral horns are not reproduced by the simulation at top left, nor are the positions of the outer spectral "shoulders," despite other similarities.***

References

1. P. D. Dietzel, R. E. Johnsen, R. Blom and H. Fjellvag, *Chem. Eur. J.*, 2008, **14**, 2389-2397.
2. P. D. C. Dietzel, R. Blom and H. Fjellvag, *Eur. J. Inorg. Chem.*, 2008, 3624-3632.
3. P. D. C. Dietzel, B. Panella, M. Hirscher, R. Blom and H. Fjellvag, *Chem. Commun.*, 2006, 959-961.
4. M. J. Katz, Z. J. Brown, Y. J. Colon, P. W. Siu, K. A. Scheidt, R. Q. Snurr, J. T. Hupp and O. K. Farha, *Chem. Commun.*, 2013, **49**, 9449-9451.
5. J. A. Rood, B. C. Noll and K. W. Henderson, *Inorg. Chem.*, 2006, **45**, 5521-5528.
6. Z. Wang, Y. Zhang, M. Kurmoo, T. Liu, S. Vilminot, B. Zhao and S. Gao, *Aust. J. Chem.*, 2006, **59**, 617-628.
7. H. E. Gottlieb, V. Kotlyar and A. Nudelman, *J. Org. Chem.*, 1997, **62**, 7512-7515.
8. C. Dybowski and G. Neue, *Prog. Nucl. Magn. Reson. Spectrosc.*, 2002, **41**, 153-170.
9. S. Antonijevic and S. Wimperis, *J. Magn. Reson.*, 2003, **164**, 343-350.
10. K. Eichele, WSolid*s*1, v.1.19.15, University of Tübingen, Tübingen, Germany, 2009.
11. R. L. Vold and G. L. Hoatson, *J. Magn. Reson.*, 2009, **198**, 57-72.
12. T. Pham, K. A. Forrest, E. H. L. Falcao, J. Eckert and B. Space, *PCCP*, 2016, **18**, 1786-1796.
13. P. D. C. Dietzel, P. A. Georgiev, J. Eckert, R. Blom, T. Strassle and T. Unruh, *Chem. Commun.*, 2010, **46**, 4962-4964.

14. J. G. Vitillo, L. Regli, S. Chavan, G. Ricchiardi, G. Spoto, P. D. C. Dietzel, S. Bordiga and A. Zecchina, *J. Am. Chem. Soc.*, 2008, **130**, 8386-8396.

15. Y. Liu, H. Kabbour, C. M. Brown, D. A. Neumann and C. C. Ahn, *Langmuir*, 2008, **24**, 4772-4777.

16. K. Sumida, M. R. Hill, S. Horike, A. Dailly and J. R. Long, *J. Am. Chem. Soc.*, 2009, **131**, 15120-15121.